Advances in Science and Technology Research Journal

Advances in Science and Technology Research Journal, 2026, 20(6), 325–342
https://doi.org/10.12913/22998624/218086
ISSN 2299-8624, License CC-BY 4.0

Received: 2026.01.12
Accepted: 2026.04.15
Published: 2026.05.01

Sustainable waste valorization of red mud steel slag geopolymers: Influence of alkalinity and carbonation curing

Vinitha Mariyappan[1], Karthiyaini Somasundaram[1*]

[1] School of Civil Engineering, Vellore Institute of Technology, Chennai 600127, India
* Corresponding author's e-mail: karthiyaini.s@vit.ac.in

ABSTRACT

The reactivity and strength of geopolymers produced from low-calcium red mud (RM) are limited under non-carbonation curing. This study investigates the effects of steel slag (SS) incorporation and carbonation curing on an RM-SS geopolymer paste. Red mud was replaced with steel slag at 20, 40,60, 80 & 100%, activated using sodium hydroxide solutions (2M, 4M, 6M & 8M) and subjected to non-carbonation and CO_2 curing. Compressive strength tests, XRD, and SEM analyses were performed to evaluate the effects. Steel slag incorporation enhances the compressive strength of non-carbonated geopolymers through C-S-H, N-A-S-H type and C-A-S-H type gel formation and matrix densification. CO_2 curing reduced the strength owing to $CaCO_3$ formation, although samples with optimal slag content maintained enhanced strength through microstructural densification. The Peak compressive strength occurred at 4M for both curing conditions, whereas lower and higher molarities showed poorer performance. XRD analysis revealed that increased SS content enhanced the amorphous hump 20–38° and gel formation. Carbonated 4M samples maintained an amorphous structure, while low-molarity mixes showed significant gel carbonation. SEM observations showed dense matrices with well-developed gels in 4M non-carbonated samples and disrupted networks with post-carbonation carbonate deposits. The incorporation of steel slag with 4M activation enhances the strength and carbonation resistance of RM-based geopolymers, offering sustainable waste valorization.

Keywords: red mud, steel slag, low calcium based geopolymer, CO_2 curing, alkali molarity, Sustainable waste, non- carbonation curing.

INTRODUCTION

Large amounts of industrial solid waste are currently produced worldwide, and they come in a variety of forms with significant variations in their physical and chemical properties, as well as unequal distribution throughout different geographical areas. These wastes are generally grouped into three main categories: silica-alumina-based solid wastes [1], calcium-based solid wastes (e.g. steel slag), and alkaline solid wastes (e.g. slag, calcium carbide slag, and red mud) [2]. The disposal of enormous amounts of industrial solid waste not only consumes valuable land and depletes natural resources but also poses major risks to environmental safety and human health [3]. As a result, developing long-term resource use strategies for managing such large amounts of garbage is critical. Harnessing their potential to produce construction materials can not only facilitate effective waste management but also yield substantial economic and social benefits by maximizing their residual value [2]. By using these waste materials, geopolymers solve the problem of disposing of garbage in landfills while also lowering the demand for ordinary Portland cement (OPC) [4]. Geopolymers minimize CO_2 emissions, use low-cost industrial waste, and increase structural performance, making them a sustainable alternative to natural resource usage [5].

Geopolymerization is a chemical process that uses alumino-silicate-rich materials as slag, fly ash [6,7], metakaolin [8,9], red mud [10] and silica fume to build a three-dimensional

alumino-silicate framework called polysialates [11]. Usually, aqueous silicates and activators such as potassium or sodium hydroxide are used in an alkaline environment for this reaction [12]. These activators interact with alumino-silicate sources to form sodium alumino-silicate hydrate (N-A-S-H) gel, the main binding phase that gives the geopolymer strength to form three-dimensional network of SiO_4 and AlO_4 tetrahedra [4].

Red mud (RM) a by-product of the extraction of alumina from bauxite ores, is rich in iron oxide and is highly alkaline because of its high concentration of silicon dioxide and aluminium oxide [13–15]. Although the alumina industry produces approximately 120 million tons of RM annually worldwide, its use is still restricted because of its high basicity and related environmental risks [16]. Nonetheless, RM-sourced GC has shown promise in the construction industry for creating tiles, blocks, and panels that provide superior thermal insulation, increased fire resistance, and reduced weight [17]. Zhang et al. [18] developed RM-FA-based geopolymers at ambient temperature and investigated the parameters that influence their mechanical characteristics, microstructure, and chemical composition. It was discovered that a higher Si/Al and Na/Al ratio resulted in a stronger geopolymer. Hu et al. examined geopolymers made with red mud (RM) and fly ash (FA). RM with C-grade FA at room temperature gave 15.2 MPa strength, while F-grade FA produced a weak geopolymer. This weakness is typical of low-calcium alkali-activated systems that lack rapid strength [19]. Yang et al. reported that red mud mixed with 20% GGBFS in geopolymer systems improves the density, lowers porosity, and promotes sustainable building by effectively using waste. After 28 days, the compressive strength increases by 83% and flexural strength by 93.75% respectively [20]. Although few studies have examined the effects of varying sodium hydroxide concentrations on the performance of red mud-based geopolymers, the majority have focused on higher NaOH molarities, such as 8–12M. Only a few experiments have examined lower NaOH molarities, such as 6M, 4M, and 2M. Rifaai et al. [21] found that NaOH concentrations below 8M provided adequate setting durations and facilitated geopolymerization up to 7M, whereas higher concentrations slowed the setting and hampered the reaction owing to repulsive forces. Chen et al. [22] found that increasing the NaOH concentration from 4M to 12M increased microstructural density and N-A-S-H gel formation while decreasing porosity, with the lowest macropore fraction observed at 6M. Previous research has demonstrated that the molarity of NaOH has a major impact on the kinetics of geopolymerization and development of strength. The compressive strength is improved by modest increases (e.g., 2M to 4M) that improve silica and alumina dissolution. Aluminosilicates may precipitate quickly at higher molarities, which restricts polymerization. This limits the microstructural development and gel formation, which frequently results in strength reduction outside the ideal range (e.g., 4M to 6M) [23].

After China, India is the world's second-largest steel producer in 2023. According to the World Steel Association, global steel output has steadily from 1.654 million tons in 2013 to 1892 million tons in 2023. Additionally, by 2030, this number is expected to rise to 1.974 million tons, according to the International Energy Agency. India produces over 19 million tons of steel slag annually in various parts of the country. This amount is expected to increase dramatically, reaching around 60 million tons by 2030 [24]. With this significant rise in steel production, the generation of steel slag has also increased drastically. This surge in slag output necessitates its sustainable utilization. Notably, the chemical composition of steel slag (SS) is similar to that of Portland cement containing CaO, SiO_2, Fe_2O_3, Al_2O_3 and MgO[25]. And it has some common mineral composition including dicalcium silicate (C_2S), tricalcium silicate (C_3S) and free calcium (f-CaO), which exhibit hydration activity. The strength of geopolymers is increased by the high CaO content in steel slag-rich binders[26]. The release of soluble Ca^{2+} ions by CaO encouraged the development of N-A-S-H and C-A-S-H gels, which enhanced the mechanical performance. Additionally, the C-A-S-H gel speeds up the geopolymerization process by acting as a nucleation site [4]. Sankar et al. found that the formation of C–S–H gels and C–(A)–S–H gels in the geopolymer structure led, to the formation of Ca- and Na-based geopolymers and accelerated the strength development of the geopolymer as the slag/fly ash ratio increased [27]. According to Niklic et al., the [28] compressive strength of fly ash geopolymers can be increased by adding up to 30% EAF slag. Additionally, the presence of C-(A)-S-H and N-A-S-H gels resulted in a denser microstructure increasing the compressive strength. Wang et al.

[29] found that adding steel slag (SS) and $Ca(OH)_2$ to low-calcium FA-RM geopolymers improved the formation of C(N)-A-S-H and C-S-H gels, enhanced the microstructure, and dramatically enhanced compressive strength, reaching 30.6 MPa after 28 days with 4 wt.% $Ca(OH)_2$ and partial RM replacement by SS. These similarities make steel slag and red mud potential alternative in construction materials providing a sustainable pathway for both waste valorization and carbon footprint reduction.

Geopolymers possess a greater ability for CO_2 curing through mechanisms such as mineral carbonation. CO_2 mineralization has been utilized in various industrial waste materials such as steel slag, red mud, blast furnace slag, cement waste, and recycled concrete waste [5]. The primary reaction product of geopolymers is a sodium aluminosilicate hydrate (N-A-S-H) gel includes calcium aluminosilicate hydrate (C-A-S-H) and calcium–sodium aluminosilicate hydrate (C-(N)-A-S-H) [30]. Geopolymers also offer a more alkaline environment than that of regular Portland cement. The C-A-S-H and C-(N)-A-S-H gels were the most exposed to carbonation reactions among these stages. However, when geopolymers are carbonated, the pH of the pore fluid drops, preventing further hydration. The decalcification of calcium-rich C-(A)-S-H and its subsequent conversion to N-A-S-H reduces gel cohesiveness and strength. In contrast, the gel structure was barely altered by the carbonation of N-A-S-H, and very little calcium carbonate crystal were formed [31]. Red mud and steel slag as reactive calcium and magnesium phases react with CO_2 and forms stable carbonates. Red mud-based geopolymer pastes activated with low molarity NaOH (0.5–2M) shown that 0.5M provided the highest strength under normal curing, while 2M performed best under carbonation. XRD and SEM revealed the development of N-A-S-H gel and sodium carbonate. Low molarity promotes geopolymerization, whereas a higher molarity facilitates CO_2 sequestration[32]. Duraisamy et al. found that mineral carbonation of red mud increases strength by 11.6% at 25 °C, 64% at 45 °C, and 50% at 65 °C, with a significant improvement observed at 45 °C [33]. Sintered red mud (SRM) revealed good carbon absorption and utilization capabilities, and the addition of 10% carbonated SRM resulted in increased strength development [34]. The carbonation of alkali-activated slag pastes in a high-humidity environment resulted in the capture of 78.8 kg of CO_2 per ton and enhanced the strength by 34.6%. This was because of the formation of $CaCO_3$ and $CaMg(CO_3)_2$, which contributed to the densification of the matrix [31]. Ladle slag as a precursor for alkali-activated materials which the ability to capture CO_2. The addition of 0.20% SDS increased CO_2 sequestration by 48% to 6.17%, which slightly decreased strength but improved overall sustainability [35].

Research gap and objective of the study

RM, a highly alkaline byproduct of alumina manufacturing, shows potential as a geopolymer precursor; however, it typically has low strength because of its low calcium and reactive silica concentration. While RM activation and its blending with different additives have been studied in the past, the combined effects of CO_2 curing, alkali molarity modification, and the addition of calcium-rich (SS) have not been thoroughly addressed. Therefore, little is known about how these factors affect microstructural evolution, strength development, and CO_2 curing efficiency. The integrated assessment of alkali molarity and carbonation curing on RM–SS-based geopolymer systems is the study's scientifically unique. It addresses carbon-efficient building techniques while offering fresh perspectives on reaction processes and performance improvement.

The objective of the study is as follows:

1. To improve the mechanical performance of low-calcium RM-based geopolymers, RM was partially replaced with calcium-rich SS in various amounts.
2. To investigate the effect of the alkali activator molarity (four levels) on geopolymerization and the subsequent mechanical and microstructural qualities.
3. To evaluate the impact of CO_2 curing, compressive strength development, and microstructural evolution.
4. To characterise hydration and reaction products using XRD and SEM techniques, and to discover correlations between microstructure and mechanical performance.
5. To promote sustainable construction materials by valorising industrial by-products (RM and SS) and evaluating the effects of CO_2 curing.

To overcome the low strength of low-calcium RM based geopolymers, calcium – rich SS replacing RM at four different molarities with

CO_2 curing. This study investigates the effects of SS and CO_2 curing on compressive strength, hydration products, and microstructure.

MATERIALS AND METHODS

Materials

RM and SS were used as the geopolymer precursors. Sodium silicate solution and sodium hydroxide pellets were used as alkali activators. SS used in this study is BOF was received from astrra chemicals. Commercial sodium silicate solution (grade N, SiO_2/Na_2O molar ratio = 2.50, density = 1.42 g/cm^3 at 20 °C, solids content: 28.5 wt% SiO_2, 12.5 wt% Na_2O, 59.0 wt% H_2O) was used as received from astrra chemicals. XRD revealed that RM contains Fe_2O_3, FeO(OH), $Al(OH)_3$, γ-AlO(OH), TiO_2, and $Na_3Al_6Si_6O_{24}(Cl_2SO_4{\cdot}CO_3)$, with minor SiO_2, whereas SS is composed of SiO_2, C_4AF, C_2S, C_3S, and small Fe_3O_4. The median diameter D_{50} of RM and SS are 36.23 µm and 5.51 µm respectively. PSD shows that RM has a broad particle size distribution, but SS has a narrower distribution with a lower median size, signifying increased reactivity as shown in Figure 1. The chemical composition of RM & SS are given in Table 1.

Sample preparation and testing methods

Geopolymer sample preparation

The geopolymer paste was prepared by sieving the red mud through a 75 µm sieve and mixing it with steel slag in different mix proportion. The SS was used as a replacement for RM by 20%, 40%, 60%, 80% and 100%. The sodium silicate to sodium hydroxide ratio was maintained at 2:1, a commonly used mid-range value near the reported optimum (≈ 2–2.5), to ensure sufficient soluble silica without excessive viscosity or efflorescence [36]. The liquid-to-binder (L/B) ratio was fixed at 0.45 to balance workability and strength. The mix design parameters were determined based on preliminary trials and literature [37]. In addition, a 100% steel slag mix was used as a reference to assess the impact of calcium-rich precursors on gel formation and mechanical performance. Sodium hydroxide concentrations of 2M, 4M, 6M and 8M were used. The alkali solution was prepared prior one day of casting. Then, the obtained mix is poured into cylindrical mould of size 6.5 × 3.00 cm. The samples were cured under two different curing conditions : non-carbonation for 7AC, 14AC & 28AC at 25 ± 2 °C, 60% RH and 7 days CO_2 curing (7CC, 7CC+ 7AC & 7CC + 21AC) at 30 ± 2 °C and 85 ± 5% relative humidity. Figure 2 shows the RM-SS based geopolymer sample preparation process & testing methods. Table 2 lists the mix proportion of geopolymer paste in weight by %.

Testing methods

The compressive strength of 6.5 × 3.0 cm cylindrical specimens was examined using a 2000 kN compression testing machine (CTM-SHIMADZU, Concreto 2000X). A loading rate of 0.5 MPa/s was used until failure, according to a protocol derived from IS 516 (2021) and ASTM C109. Each mixture was evaluated with three specimens. Microstructural examination was performed using SEM at 10,000× magnification for the non-carbonated and CO_2 cured samples. XRD was done on powdered samples using a RIGAKU Smart Lab 3 kW (CuKα, 40 kV, 40 mA) over 2θ = 5–80° with 0.02° intervals. Phases were detected using X′Pert High Score Plus and spectra were viewed using OriginPro.

RESULTS AND DISCUSSION

Compressive strength

Non-carbonated RM- SS based geopolymer paste

The compressive strengths of red mud (RM) and steel slag (SS)-based geopolymer pastes were cast using different molarities (2M, 4M, 6M, and

Table 1. Chemical composition and physical properties of raw materials

Raw materials	Chemical composition in (wt%)						Physical properties		
	SiO_2	Al_2O_3	CaO	Fe_2O_3	MgO	SO_3	D_{10} (µm)	D_{50} (µm)	D_{90} (µm)
RM	19.27	35.14	2.325	29.73	0.94	0.36	10.35	36.23	88.87
SS	38.68	20.74	24.89	0.31	12.00	1.39	1.54	5.51	11.95

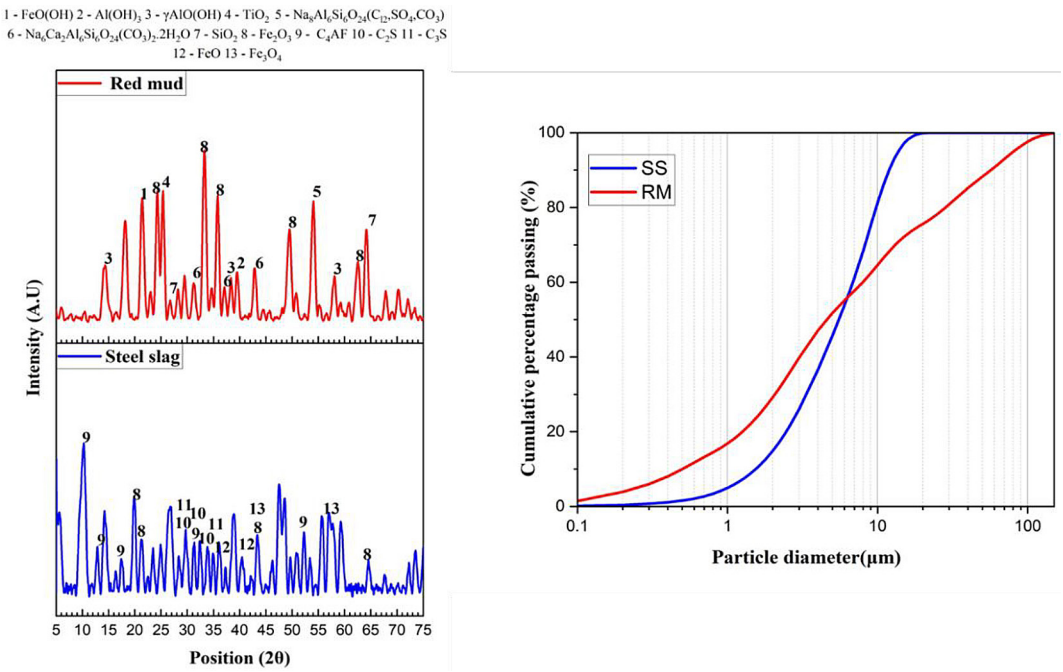

Figure 1. Particle size distribution and XRD of raw RM and SS

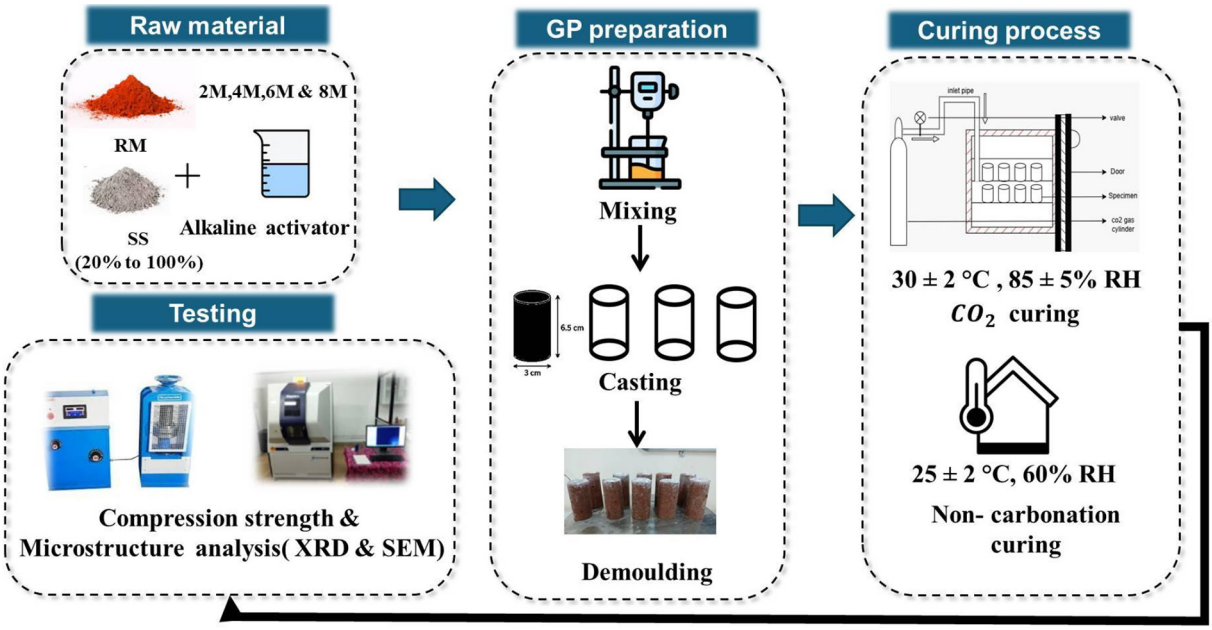

Figure 2. RM-SS based geopolymer sample preparation process & testing methods

8M) and progressively replaced with red mud (0–80%) without carbonation as shown in Figure 3. The results show that both the alkaline activator concentration and RM-SS ratio play a significant role in the mechanical properties of the mixes. At 2M, with increasing SS content, the compressive strength gradually increased and peaked in 2NC 4 and 2NC 5. Because of its high calcium concentration, it enhances the formation of C-(A)-S-H type gel and C-S-H in addition to the N-A-S-H type gel from RM. SS plays a significant role in improving matrix densification and strength development. Calcium – rich steel slag significantly improves geopolymerization [38]. Additionally, Sun et al. discovered that alkali-activated SS exhibits hydration processes and products comparable to cement. The inclusion of SS can significantly increase hydration

Table 2. Mix proportion of geopolymer paste in (%)

Curing	Specification	RM	SS	Molarity	Liquid / binder ratio	Alkaline activator module
Non carbonation	2NC 1	80	20	2M	0.45	2
	2NC 2	60	40	2M	0.45	2
	2NC 3	40	60	2M	0.45	2
	2NC 4	20	80	2M	0.45	2
	2NC 5	0	100	2M	0.45	2
	4NC 1	80	20	4M	0.45	2
	4NC 2	60	40	4M	0.45	2
	4NC 3	40	60	4M	0.45	2
	4NC 4	20	80	4M	0.45	2
	4NC 5	0	100	4M	0.45	2
	6NC 1	80	20	6M	0.45	2
	6NC 2	60	40	6M	0.45	2
	6NC 3	40	60	6M	0.45	2
	6NC 4	20	80	6M	0.45	2
	6NC 5	0	100	6M	0.45	2
	8NC 1	80	20	8M	0.45	2
	8NC 2	60	40	8M	0.45	2
	8NC 3	40	60	8M	0.45	2
	8NC 4	20	80	8M	0.45	2
	8NC 5	0	100	8M	0.45	2
CO_2 curing	2C 1	80	20	2M	0.45	2
	2C 2	60	40	2M	0.45	2
	2C 3	40	60	2M	0.45	2
	2C 4	20	80	2M	0.45	2
	2C 5	0	100	2M	0.45	2
	4C 1	80	20	4M	0.45	2
	4C 2	60	40	4M	0.45	2
	4C 3	40	60	4M	0.45	2
	4C 4	20	80	4M	0.45	2
	4C 5	0	100	4M	0.45	2
	6C 1	80	20	6M	0.45	2
	6C 2	60	40	6M	0.45	2
	6C 3	40	60	6M	0.45	2
	6C 4	20	80	6M	0.45	2
	6C 5	0	100	6M	0.45	2
	8C 1	80	20	8M	0.45	2
	8C 2	60	40	8M	0.45	2
	8C 3	40	60	8M	0.45	2
	8C 4	20	80	8M	0.45	2
	8C 5	0	100	8M	0.45	2

Note: *RM – red mud, SS – steel slag, NC – non-carbonated, C – CO_2 cured. Mix codes: first digit = NaOH molarity (2 or 4 M), NC/C = non-carbonated or carbonated condition, final number = Mix sequence*.

activity of the geopolymer system and encourage the formation of additional hydration products, including C-S-H type gel in the matrix [39]. At 4M, the 4NC 2 mix showed the highest strength. This suggests that a balanced ratio of RM and SS promotes a synergistic effect by enhancing both dissolution and gel formation, which leads to the coexistence of C-(A)-S-H and N-A-S-H type

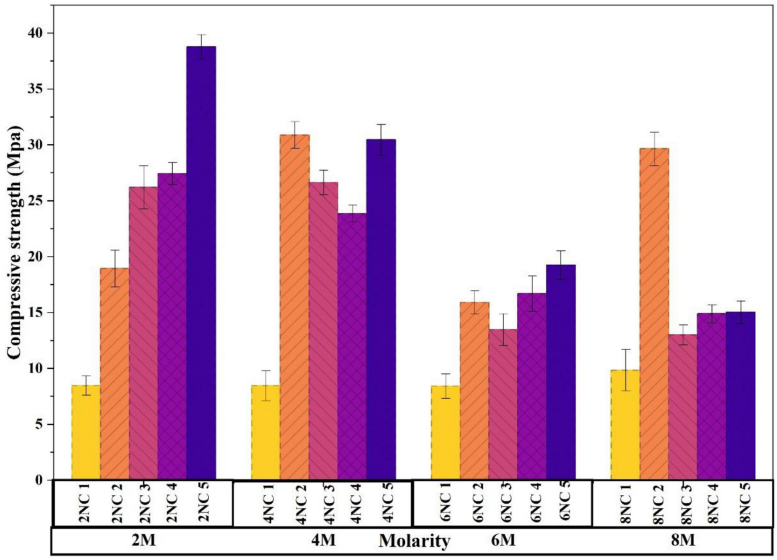

Figure 3. Compressive strength of non- carbonated RM-SS based geopolymer paste

gels, leads in a denser and stronger microstructure [40]. Slag promotes C-S-H gel formation in low-alkaline environments. Because red mud is alkaline in nature, it does not require a high molar alkaline activator. Therefore, mixing slag with red mud increases the possibility of C-S-H gel formation at low molarity. This could be a result of the high strength of the paste at a low molarity [23]. The compressive strength decreased for all mixes as the molarity increased to 6M. This reduction in strength owing to excessive alkalinity, causes rapid precipitation of the reaction product, with incomplete geopolymerization and formation of microcracks. Chen et al. (2024) also found that increased molarity prevents the development of long-term strength in RM-slag based geopolymers and hinders gel formation[41]. The mix with higher SS content 6NC 4 and 6NC 5 still has better strength compared with RM rich mixes, suggesting that calcium plays a role in enhancing matrix stability. Comparing 8M to 6M, the compressive strength exhibited a slight recovery, with 8NC 2. This suggests that the effectiveness of geopolymerization increased when a moderate alkalinity and an ideal RM–SS ratio are combined. However, pore development and structural flaws can result from an excessively high alkalinity [32] [23,42]. The optimal ratio of RM–SS geopolymers is a promising sustainable substitute for traditional binders because it produces a denser microstructure and superior compressive strength when red mud and steel slag are optimally balanced, especially at moderate activator molarities.

CO_2 cured red mud steel slag based geopolymer paste

The Figure 4 shows the compressive strength of the geopolymer pastes from RM and SS with different molarity concentrations under CO_2 curing. At 2M & 4M, increasing the SS content generally enhanced the compressive strength of the RM-SS based geopolymers, except for 2C 5 and 4C 5. 2C 4 exhibited the highest compressive strength due to its calcium content. Adequate calcium from slag contributes to the formation of C-A-S-H type gel, while 20% RM leads to the formation of N-A-S-H type gel. When exposed to CO_2, dissolved calcium reacts to form $CaCO_3$, which is found within the pores. These pores are filled with $CaCO_3$, which boosts the strength, densifies the matrix, and reduces porosity[43,44]. This advantageous carbonation predominates at low to moderate molarities (2–4M) with a larger slag content (>50% SS), where $CaCO_3$ precipitation refines pores without excessive C-(A)-S-H decalcification[45]. At higher molarities (6M and 8M), the increasing OH^- concentration accelerates dissolution and results in fast gel precipitation. Although this can increase the early strength gain in the 6M, the reaction products tend to become coarser and non-uniform, with entrapped porosity and microcracks that affect long-term performance[46]. Carbonation changes are harmful because high alkalinity (>6M) encourages C-(A)-S-H decalcification, where $CaCO_3$ synthesis competes with gel binding for Ca^{2+} ions, resulting in silica gel formation, shrinkage, and a reduction in strength, which is especially noticeable.

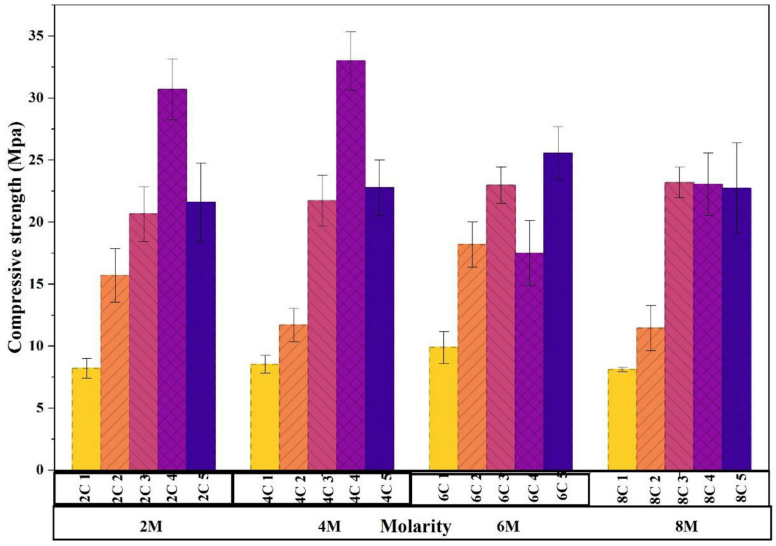

Figure 4. Compressive strength of RM-SS based geopolymer paste to CO_2 curing

Carbonation causes lots of Ca species and free alkalis to react with the CO_2. However, some calcium is absorbed into unstable phases that decalcify, leading to shrinkage, microcracking, and structural integrity loss [47]. Strength tends to decline or remain inconsistent when compared to 2M & 4M. At 8M, the reaction becomes much more aggressive, resulting in very disordered gel networks and severe defects due to fast gelation and shrinkage [48]. Although a strong alkalinity initially protects against CO_2 entry, carbonation still destabilizes C-(A)-S-H type gel, leading to efflorescence and pore coarsening. $CaCO_3$ generated was limited to minor densification [49]. As a result, mixtures activated with 8M NaOH often exhibit poor mechanical performance and durability under carbonation.

XRD analysis

Non-carbonated RM-SS based geopolymer paste

XRD analysis of the non-carbonated RM-SS based geopolymer cured for 28 days with varying molarity is shown in Figure 5. A broad hump in the 20–38° range was seen in all samples, indicating the production of an amorphous aluminosilicate gel phase such as C–A–S–H type gel(calcium aluminosilicate hydrate) and N–A–S–H type gel (sodium aluminosilicate hydrate). These amorphous phases were the main binding products of geopolymerization [29]. In 2M, 2NC 1 shows sharper and more intense unreacted minerals such as hematite, quartz, wustite, magnetite, boehmite, and gibbsite as crystalline peaks, indicating partial crystallinity and low gel content. The particularly noticeable amorphous hump in 2NC 4 indicates a larger gel content and better geopolymerization under these circumstances. In contrast, 2NC 5 has a broad amorphous backdrop and decreased crystalline intensity, indicating the creation of a more polymerized network.

In 4M, sharp crystalline peaks remain in 4NC 1, with little broad hump found between 20–35°, indicating negligible amorphous gel formation. A diffuse hump in the 20–35° range is still visible in 4NC 5, suggesting the coexistence of an amorphous geopolymer gel with crystalline products, despite the presence of a very intense peak at around 29°, which corresponds to calcite or a comparable Ca-containing phase. Conversely, 4NC 2 had the highest amorphous phase among the three samples, with lower peak intensities and, a more noticeable hump in the 20–35°. In 6M, 6NC 1 had extremely sharp peaks of quartz, calcite, hematite, and magnetite, with only a slight amorphous hump, indicating high crystallinity. Strong calcite peaks predominate in 6NC 4, where the amorphous signal is partially reduced, suggesting less gel formation. However, 6NC 5 confirmed a larger amorphous gel content with lower peak intensities, a broad hump at 20–35°, and an increased baseline. In 8M, 8NC 1 had more crystalline peaks with fewer C-A-S-H & N-A-S-H type gels. However, 8NC 2 confirms a slightly more amorphous gel than 8NC 1 at around 20–35°. As the amount of slag increased to 80 to 100%, secondary peaks of calcite ($CaCO_3$), calcium silicate hydrate (C–S–H) gel, and alite (Ca_3SiO_4) were

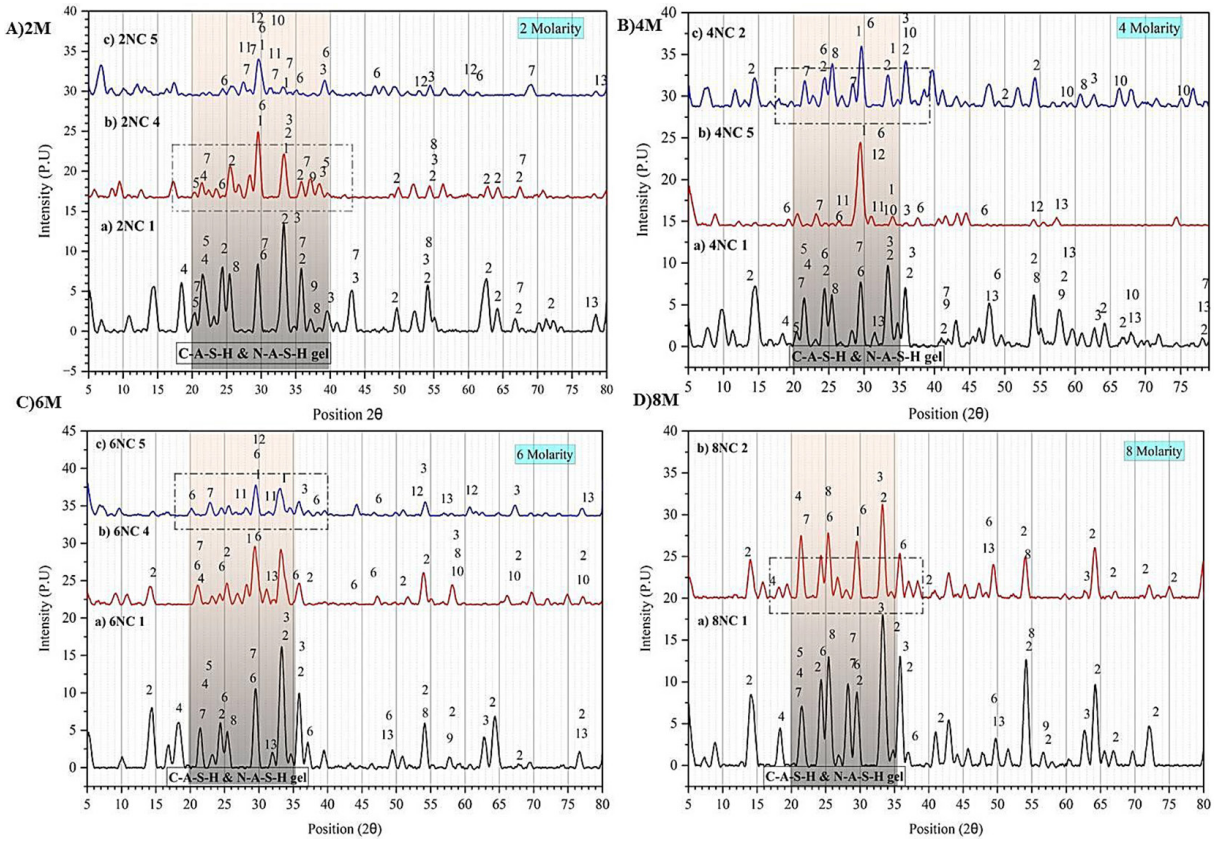

Figure 5. XRD pattern of the non-carbonated RM-SS based geopolymer paste: A) 2M, B) 4M, C) 6M, D) 8M. 1 – CSH, 2 – hematite, 3 – wustite, 4 – boehmite, 5 – gibbsite, 6 – calcite, 7 – quartz, 8 – titanium oxide, 9 – periclase, 10 – magnetite, 11 – alite, 12 – calcium iron oxide, 13 – gehlenite

observed. Additionally, previous research has shown that C-S-H gels are the primary binding phase of geopolymer slag materials [29,50]. The peaks around 29.68° & 49.5° belongs to calcite and the Ca^{2+} present in the steel slag reacts with atmospheric CO_2 air forms $CaCO_3$ [51] formed more in 2NC 4, 2NC 5, 4NC 5, 6NC 4, 6NC 5 and 8NC 2. Samples with lower molarity such as 2M and 4M promote amorphous phase formation, enhancing the early compressive strength through effective gel development and network polymerization. Conversely, higher molarity (6M & 8M) levels lead to distinct crystalline phases, potentially hindering additional gel formation and strength is also reduced [18].

XRD of RM-SS based geopolymer paste subjected to CO_2 curing

Figure 6 presents the XRD analysis of the RM-SS-based geopolymer paste subjected to CO_2 curing for 28 days, with varying molarities. In samples 2C 1, 4C 1, 6C 1, and 8C 1, there were more crystalline phases, including hematite, quartz, titanium oxide, periclase, magnetite, and brownmillerite, which acted as inert and filler materials in all RM 80% & SS 20% mixes. A broad hump in the 20–40° range was observed in all samples, indicating the formation of an amorphous aluminosilicate gel phase, such as C–A–S–H type gel (calcium aluminosilicate hydrate) and N–A–S–H type gel (sodium aluminosilicate hydrate) [52]. In 2M, sample 2C 5 shows slight amorphous phase gel formation along with some calcite and periclase, while 2C 4 exhibits a broad amorphous hump of C-A-S-H & N-A-S-H type gel around 20–40°, along with more calcite. Natron is formed from the reaction of Na^+ ions in red mud with CO_2. Unreacted materials were also present in 2C 5, but the peak intensity was less than that in 2C 1 & 2C 5. In 4M, 4C 1 displays sharp crystalline phases indicating that all the raw materials are not dissolved properly and a small amount of amorphous phase is formed. While 4C 4 has an increase in the amorphous phase compared to 4C 1, it indicates that a strong amorphous phase is observed owing to an increase in molarities to 4M. In 2C 4 and 4C 4, the steel slag content increased to 80%, and

calcium present in the slag reacted with CO_2 curing to form calcite ($CaCO_3$) [53,54]. Calcite peaks were stronger at 4C 4 & 2C4, owing to CO_2 curing. Calcite at 29.4° 2θ in 2–4M high-slag mixes (2C4, 4C4) demonstrates advantageous pore-filling; silica at ~22° 2θ alongside calcite in 6–8M mixes indicates C-(A)-S-H decalcification from Ca^{2+} competition [55]. In 6M, 6C 1 displayed more pronounced peaks between 20° and 40°, indicating a significant amount of crystalline material. Conversely, in 6C 5 the shaded hump area suggests the presence of amorphous C-A-S-H and N-A-S-H gels, although these gels coexisted with unreacted crystalline components. The presence of the crystalline peaks suggests that the geopolymerization process is not yet fully complete.

In 8M, 8C 1 has more unreacted minerals. This is indicated by clear crystal peaks and a weaker non-crystal area. 8C 5 shows more geopolymerization and gel formation. This was observed in the weaker crystal peaks and stronger gel areas. Out of the three, 8C 4 had the most gel phase. It has the highest non-crystal peak and weakest crystal peaks in the given area [56]. During CO_2 curing, calcium and free alkalis react with CO_2. Some calcium forms unstable parts that deteriorate later, causing shrinkage and crackings. The $CaCO_3$ formed added a minimal density without significant strengthening. Consequently, the compressive strength at 6M and 8M decreases compared that to lower concentrations (2M and 4M).

SEM analysis

Non- carbonated RM-SS based geopolymer paste

After 28 days of curing at ambient temperature, SEM was employed to analyze the morphological properties of the geopolymers made from RM and SS. Figure 7 shows the corresponding micrographs of the synthesized geopolymer paste. In 2NC 1 and 2NC 4, a heterogeneous microstructure was revealed, characterized by loosely packed unreacted particles, voids, and microcracks on one side, and denser C-(A)-S-H type and N-A-S-H type gels on the other. 2NC 1 indicates potential weakness, whereas 2NC 4 contains calcite and C-S-H structures. However,

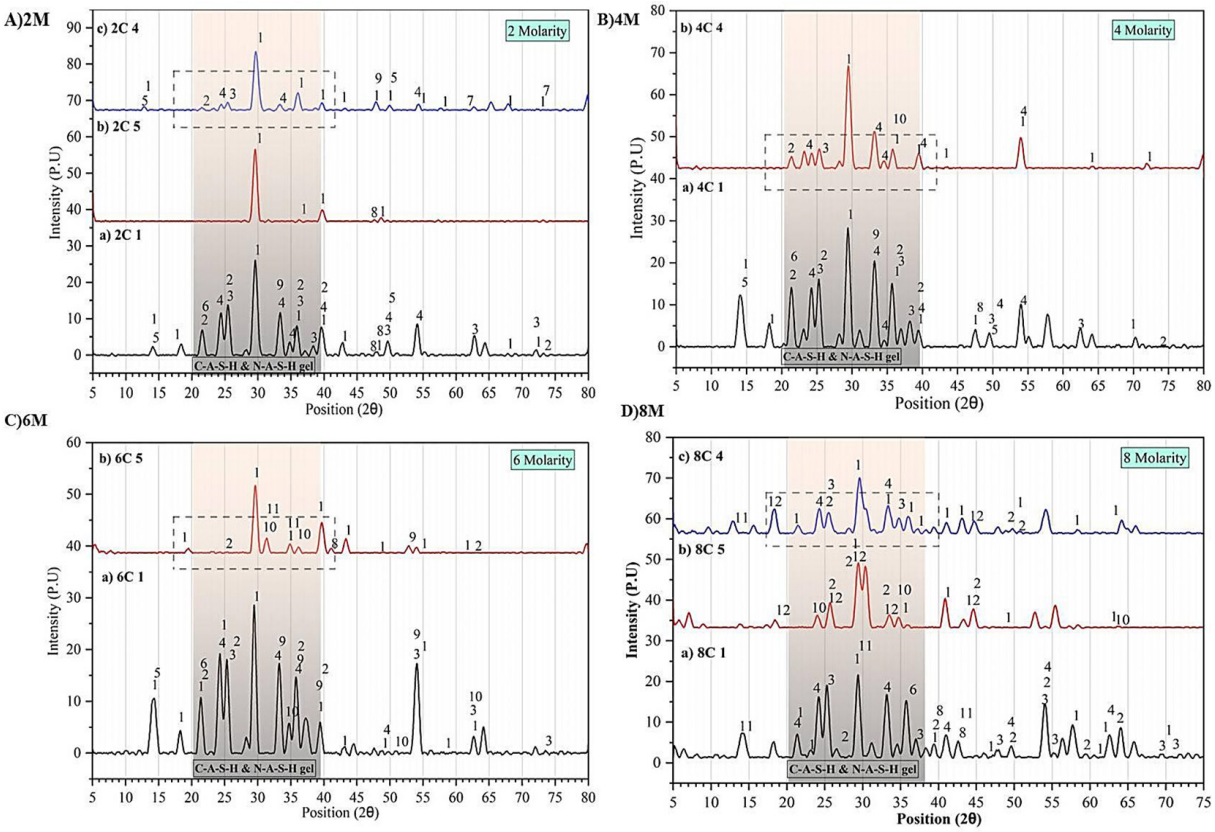

Figure 6. XRD of RM-SS based geopolymer paste subjected to CO_2 curing: A) 2M, B) 4M, C) 6M, D) 8M. 1 – calcite, 2– quartz, 3 – titanium oxide, 4 – hematite, 5 – natron, 6 – gibbsite, 7 – calcium iron silicate, 8 – periclase, 9 –brownmillerite, 10 – magnetite, 11 – bohmite, 12 – gehlenite

2NC 5 exhibited a denser and more complete C-A-S-H type and N-A-S-H type gel, along with C-S-H, resulting in improved strength. Similar to 2NC 1, 4NC 1 shows partial gel formation with more unreacted materials in the granular and porous regions. In 4NC 5, an uneven geopolymer microstructure was observed, where unreacted particles were embedded within the binding matrix formed by the C-A-S-H type gel and partial disintegration. Comparing 2NC 5 and 4NC 2 reveals dual gel formation, such as C-A-S-H type and N-A-S-H type gel, with embedded C-S-H and more unreacted materials acting as fillers in pores, limiting the reactivity of the materials. In 6NC 1, there was less gel formation with more unreacted and loose particles, resulting in reduced strength. A more packed and compact structure was seen in 6NC 4, with more microcracks and pores. In contrast, 6NC 5 had a compacted structure with fewer microcracks and unreacted particles than 6NC 4, and denser C-A-S-H type and C-S-H structures were formed. Both 8NC 1 and 8NC 2 contain more loose particles and unreacted materials, with very little gel formation, resulting in significantly reduced strength compared to other samples. At low molarity, an increase in the RM content led to partially compacted gel formation with unreacted materials. Conversely, at higher molarities and with increased RM content, proper gel formation was absent, resulting in more unreacted materials. A higher molarity can cause rapid geopolymerization, which may inhibit gel formation and lead to excess alkali in the matrix [23]. When the SS content was increased to 100% at lower molarities, the calcium-rich slag formed calcite and C-S-H along with gel formation. However, at higher molarities with increased SS content, the structure becomes coarser and more heterogeneous. Excess alkalinity results in more pores owing to the hindered gel formation [42]. Geopolymers synthesized from calcium silicate sources exhibit decreased compressive strength in alkaline environments, as most calcium precipitates as calcium hydroxide and less C-S-H gel forms. Consequently, the strength of the calcium-rich geopolymer was lower owing to the increased alkalinity of the matrix [23].

SEM of RM-SS based geopolymer paste to CO_2 curing

The SEM analysis was carried out to investigate the microstructure of the RM-SS based geopolymer paste with varying molarity under CO_2 curing, as shown in Figure 8. The SEM image indicates that in (a) 2C 1 and (d) 4C 1, at low molarity, there is an increase in red mud content, resulting in more unreacted red mud particles and pores, along with some gel formations and natron due to CO_2 curing. The geopolymer gel network remains weak at low molarity, and carbonation obstructs pores, reducing strength due to insufficient geopolymerization. The pore structure was further altered, and gel growth was restricted by the formation of sodium carbonates, or natron [57]. In contrast, at higher molarities such as (f) 6C 1 and (h) 8C 1, there is a heterogeneous formation with pores, and some natrons are filled with pores. Faster and more gel formation occurs at high molarity, but carbonation may prematurely convert these gels into carbonate phases, weakening the binding structure and diminishing the overall strength [32,57]. In (c) 2C 4 and (e) 4C 4, where the steel slag content increases to 80% at a lower molarity, there is a denser C-A-S-H type and N-A-S-H type gel with more calcite and some angular unreacted materials. Complete dissolution and geopolymerization were observed. Because calcite and other carbonation products can precipitate within pores due to slower geopolymerization, carbonation curing can enhance strength under low molarity conditions, densify the microstructure and improv durability and compressive strength [58]. Conversely, at 8C 4, gel formation with more angular raw materials is incorporated into the gel, resulting in reduced strength compared with lower molarity.

COMPARATIVE INFLUENCE OF CARBONATED AND NON-CARBONATED CONDITIONS ON GEOPOLYMER PERFORMANCE

Compressive strength

Effect of steel slag content

The addition of steel slag (SS) had a major impact on the compressive strength development of the RM -based geopolymer paste under both CO_2 and non-carbonated curing. Beyond its chemical contribution, the smaller particle size distribution (PSD) of steel slag allows for better interstitial filling between binder and larger red mud particles, which improves particle packing

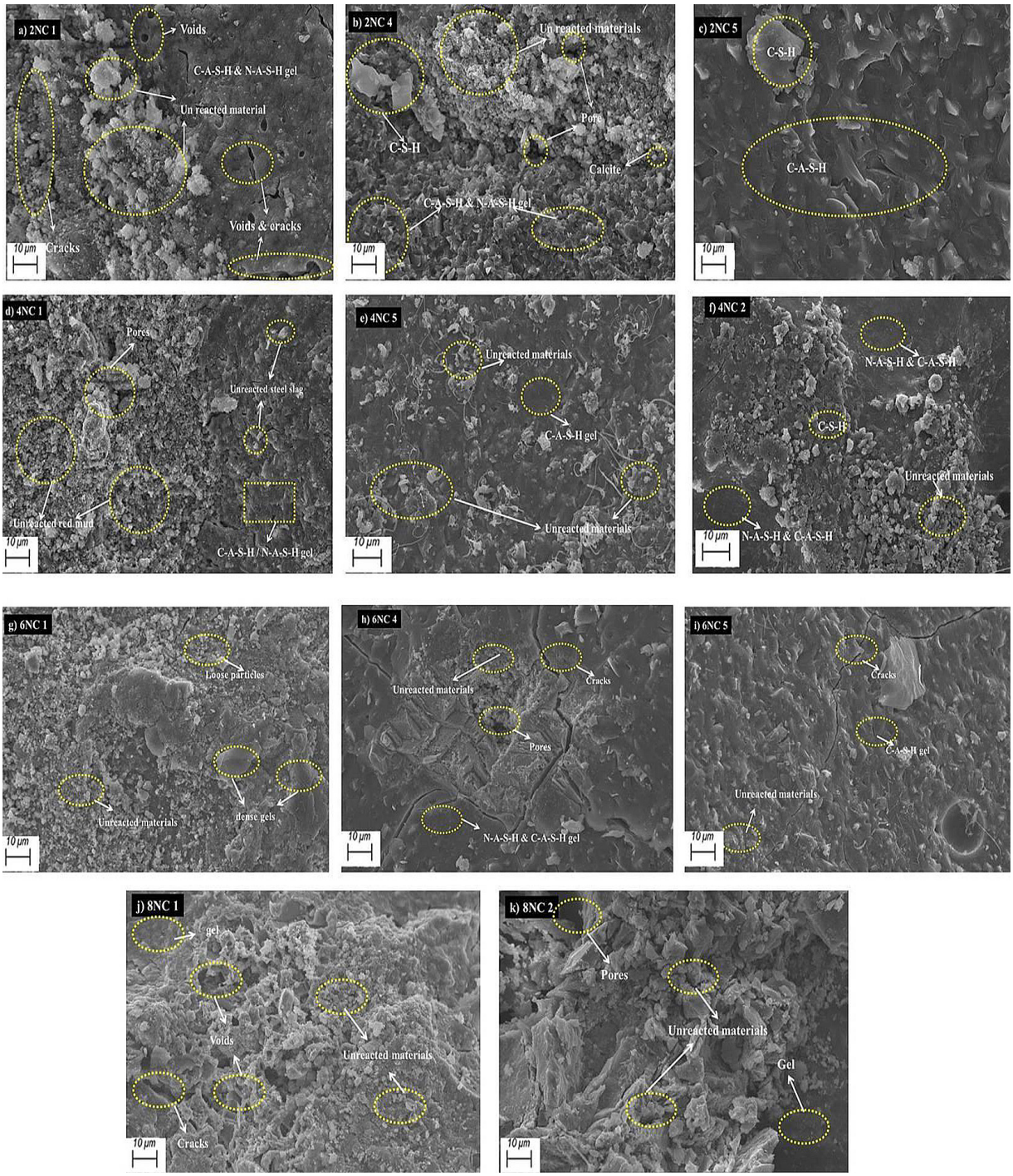

Figure 7. Non-carbonated RM-SS based geopolymer paste a) 2NC 1 b) 2NC 4 c) 2NC 5 d) 4NC 1 e) 4NC 5

and creates a denser microstructure. Compared to matrices dominated by coarser fillers, this optimized packing improves load transfer and reduces internal voids, resulting in a 15–30% increase in compressive strength in blended systems [59]. Chemically, the presence of SS increases the reactivity of the system because of its calcium- and silicate-rich composition, promoting the production of new binding phases such as C-A-S-H type and C-S-H gels in addition to the normal N-A-S-H type gel network [29]. In non-carbonation curing, 2NC 5 & 4NC 5 mixes with higher amount of steel slag have increased strengths compared to those with lower slag content. The synergistic effect of steel slag and red mud is responsible for this improvement, because the Ca^{2+} ions in the slag speed up condensation processes and densify the matrix [60]. The mixes with the optimal SS proportion at 2M and 4M NaOH had maximum compressive

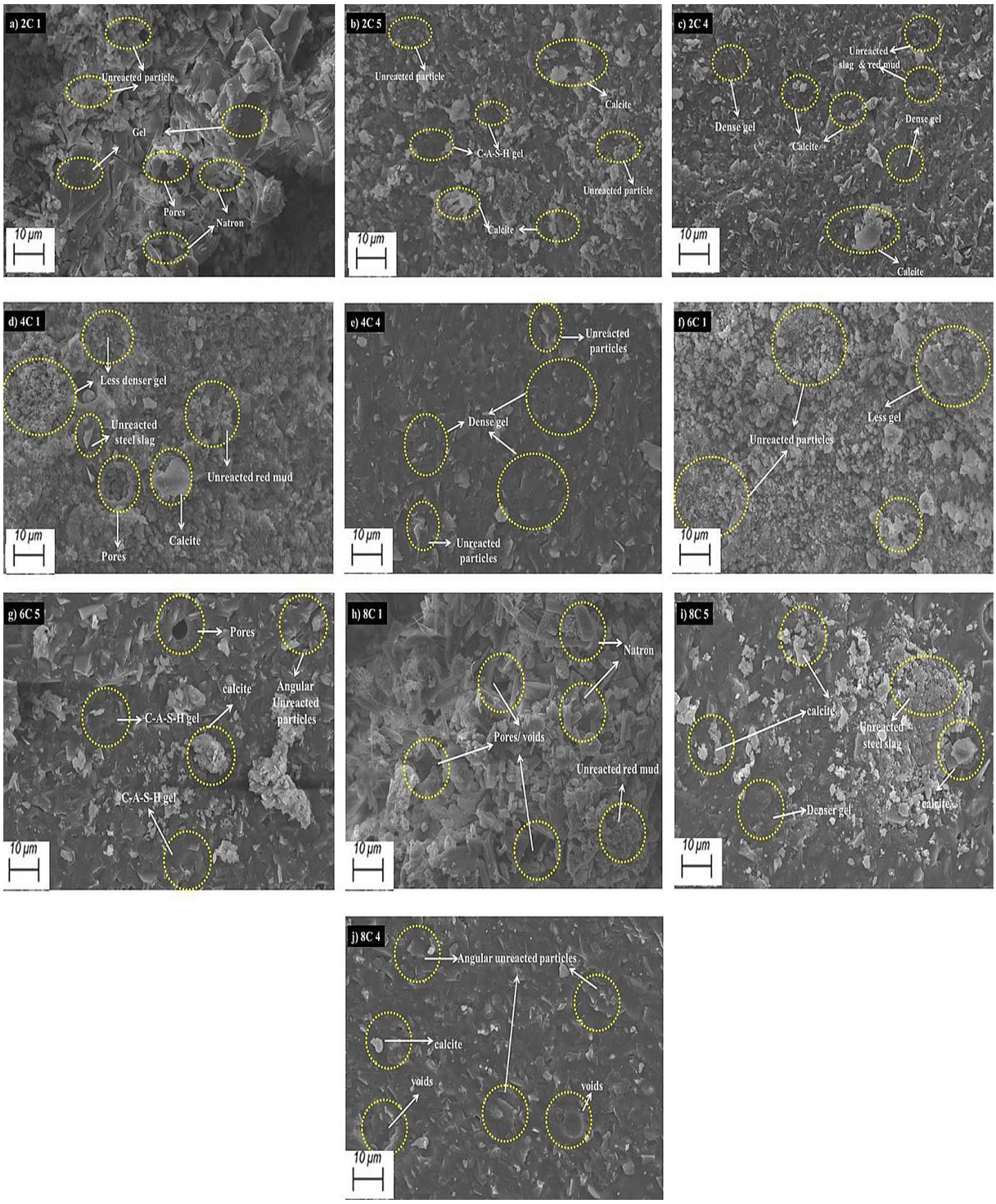

Figure 8. SEM of RM-SS based geopolymer paste under CO_2 curing: a) 2C 1, b) 2C 5, c) 2C 4, d) 4C 1, e) 4C 4, f) 6C 1, g) 6C 5, h) 8C 1, i) 8C 5, j) 8C 4

strengths of approximately 40 MPa and 32 MPa, respectively, exhibiting effective geopolymerization and gel interlocking. However, with CO_2 curing shown in Figure 3, the positive effect of SS was partially countered by carbonation-induced reactions. The Ca-rich slag phases reacted with CO_2 to generate $CaCO_3$, resulting in pore modification but lowering the available Ca^{2+} for C-A-S-H type gel formation [61]. As a result, CO_2 cured samples exhibited slightly lower strengths than non-carbonated samples. Despite this, 4C 4 and 2C 4 mixes with minimal SS content retained relatively superior strength, suggesting that SS increased the carbonation resistance of the red mud-based geopolymer via microstructural densification. Overall, the steel

slag increases strength under non-carbonation curing and slightly reduces improvement in carbonated environment by reducing the fine turning pore structure and matrix densification.

Effect of molarity

The molarity of the alkaline activator had a significant impact on the compressive strength of the RM-SS-based geopolymer paste. Figures 3 and 4 indicate that compressive strength gains with molarity up to 4M after gradually decreasing for both CO_2 cured and non-carbonated specimens. At 2M, partial dissolution of aluminosilicate species caused insufficient geopolymer gel formation, resulting in decreased strength. Under both curing circumstances, the 4M mix produced the highest strength, indicating that this molarity offered the best possible balance between the rates of dissolution and condensation. The molarity increased to 6M & 8M. Increased alkalinity may cause the soluble silica and alumina to dissolve more quickly from the precursor. Excess OH^- ions might cause rapid precipitation of aluminosilicates, hindering geopolymerization in later stages. Higher molarity may result in a decrease in strength [62]. Under CO_2 curing, however, the 4M mix lost 15–25% of its strength because sodium carbonate (Na_2CO_3) was formed in the pore network and the alkalis were partially neutralized. As molarity increased to 6M and 8M, compressive strength decreased, probably due to extra Na^+ ions causing gel separation and efflorescence [63]. Carbonation reduced strength differences in high-molarity samples compared with non-carbonated curing. This suggests that the denser matrix inhibited CO_2 diffusion but did not increase gel binding. Geopolymerization and strength were best at moderate alkalinity levels (around 4M). Both low and very high levels slowed the reaction. Carbonation weakened the gel structure at all levels, especially in lower, more porous materials.

Mineral phase

The crystalline and amorphous phases found in the RM-SS based geopolymer paste under both CO_2 cured and non-carbonated conditions were identified using X-ray diffraction (XRD) research. This comparison provides insight into the impact of geopolymerization, phase evolution, and carbonation's on the structural integrity of the binder matrix. In carbonation curing as red mud increased, the strength of the amorphous hump decreased, indicating reduced geopolymer gel formation and geopolymerization. Stronger peaks of hematite (Fe_2O_3), anatase (TiO_2), gibbsite ($Al(OH)_3$), some wustite (FeO), magnetite and quartz (SiO_2) indicated more unreacted crystals. Red mud adds minerals that react minimally [64]. The amorphous aluminosilicate gel exhibited a broad hump around 20–38°. The amorphous hump became more intense as the amount of steel slag increased, suggesting improved geopolymerization and the creation of C-S-H, N–A–S–H type and C–A–S–H type gels. Steel slag resulted in a denser amorphous structure, as indicated by the decrease in crystalline peaks from calcite, hematite, and quartz [29]. A low alkalinity (4M NaOH) resulted in a stronger amorphous hump and a lower intensity of unreacted crystalline phases, indicating improved geopolymerization. During CO_2 curing, carbonate peaks (Na_2CO_3, $CaCO_3$) were strengthened with more red mud. The weaker amorphous hump showed carbonation consumed geopolymer gel, weakening the aluminosilicate network and potentially a decrease in mechanical strength [65]. Some amorphous structure were retained upon carbonation at moderate molarity (4M), whereas lower molarity samples showed practically full gel transformation into carbonates. High molarity samples also showed carbonate peaks, although they were slightly more amorphous due to the initial stronger gel formation.

Microstructural analysis

The SEM images highlight the significant microstructural variations between non-carbonated and CO_2 cured red mud–steel slag geopolymer pastes. In the non-carbonated specimens, the matrix was relatively compact and uniform, featuring well-developed C–A–S–H type and N–A–S–H type gels, minimal porosity, and only a few unreacted particles of red mud or steel slag, especially in mixtures with a higher slag content [58]. In contrast, the CO_2 cured samples showed a disrupted gel network, with increased pores and voids, and the presence of carbonate crystals such as calcite and natron, which partially replaced or obstructed gel formation. Micro-cracks are more common, and there is a higher amount of unreacted material, suggesting that carbonation hinders complete geopolymerization [40,66]. Furthermore, the molarity of the alkali solution has a major influence on the microstructure of

CO_2 cured and non-carbonated: at low molarities (2M), the matrix is rather porous with partial gel formation, whereas moderate molarity (4M) promotes a more compact and continuous gel structure. A higher molarity (6–8M) results in localized agglomeration and some unreacted particles, indicating that excessive alkalinity may impede uniform geopolymerization [40]. A dense and well-connected N-A-S-H gel network with optimal strength is produced at moderate NaOH molarity (4M) when sufficient OH^- availability permits balanced dissolution and controlled polycondensation. However, excessive alkalinity at 8 M causes flash precipitation because silicate and aluminate species quickly become supersaturated. This disrupts gel formation, increases internal stresses, and encourages microcracking and pore coarsening, all of which eventually weaken the binder's microstructure and strength [67]. Overall, the combined effect of carbonation and alkali molarity demonstrates that intermediate molarity during non-carbonated curing results in the densest microstructure, whereas carbonation and extreme molarities degrade matrix integrity. A higher steel slag content promotes gel formation in both curing situations. Nevertheless, the negative microstructural effects of carbonation, such as lower gel continuity, increased porosity, and crystalline deposits, are evident, correlating to the reported loss in mechanical performance during carbonated curing. SEM observations align with XRD findings and compressive strength: dense, continuous C-A-S-H type gels in 2C4/4C4 (4M, high SS) matched the peak strength and calcite at 29.4° 2θ, while microcracked, porous matrices in 6C5/8C5 (6–8M) align with Q^4 silica peaks at ~22° 2θ and strength decline from C-(A)-S-H type gels decalcification. This microstructure-mechanical coupling demonstrates that CO_2 curing improves low-molarity/high-slag mixtures while having a negative impact on high-molarity mixes.

CONCLUSIONS

This research shows that adding calcium-rich steel slag significantly increases the compressive strength of red mud-based geopolymers under non-carbonated curing by densifying the matrix and encouraging the production of C–A–S–H type and C–S–H gels. Although mixes with appropriate slag concentration, especially at 2C4 and 4C4, retain increased strength and carbonation resistance due to microstructural densification, CO_2 curing lowers this strength enhancement owing to the consumption of Ca^{2+} ions through $CaCO_3$ production. While lower molarities led to insufficient gel formation and higher molarities caused rapid precipitation and agglomeration, 4M showed the highest compressive strength among the investigated alkali molarities under both CO_2 cured and non-carbonated conditions, suggesting an ideal balance between precursor dissolution and gel condensation. All molarities experienced strength reduction because of CO_2, with porous, low-molarity systems experiencing more noticeable losses. In contrast, the 4M mixes displayed comparatively less strength loss despite partial Na_2CO_3 production. Crystalline and amorphous phases coexisted in RM–SS geopolymers, according to XRD results. Increasing the steel slag content increased the amorphous hump between 20° and 38° and encouraged the production of C–S–H, N–A–S–H type, and C–A–S–H type gels while decreasing unreacted crystalline phases. Higher red mud concentration, on the other hand, exacerbated carbonate formation during CO_2 cured and increased crystalline phases such hematite, anatase, gibbsite, and quartz, weakening gel networks. While low molarity caused substantial gel conversion to carbonates and high molarity only demonstrated partial amorphous retention, CO_2 cured samples at 4M preserved a relatively greater amorphous structure. Even at higher steel slag contents, carbonation caused gel degradation, increased porosity, microcracking, and carbonate crystal formation, which ultimately reduced matrix integrity. Microstructural observations further confirmed that non-carbonated samples displayed a dense and homogeneous matrix at 4M.

Acknowledgment

The authors express their gratitude to the Vellore Institute of Technology, Chennai, for the necessary support in implementing this work. Additionally, we would like to express our deep gratitude to Dr. M. Shanmugasundaram, Associate Professor, School of Civil Engineering, Vellore Institute of Technology, Chennai, for his valuable insights that significantly aided in the completion of this study.

REFERENCES

1. Suprakash AS, Karthiyaini S, Shanmugasundaram M. Future and scope for development of calcium and silica rich supplementary blends on properties of self-compacting concrete - A comparative review. Journal of Materials Research and Technology. Elsevier Editora Ltda; 2021; 15, 5662–81.
2. Li J, Hou Q, Zhang X, Zhang X. Microbial-induced mineral carbonation: A promising approach for improving Carbon sequestration and performance of steel slag for its engineering utilization. Developments in the Built Environment. 2025 Mar 1;21.
3. Zhai B, Zheng X, Zhang H, Ran J, Dang Y, Huang Y, et al. Enhanced CO_2 sequestration in red mud slurry via ultrasonic pretreatment. Sep Purif Technol. 2025 Jul 8;360.
4. Kishore K, Sheikh MN, Hadi MNS. A critical analysis of electric arc furnace (EAF) slag for sustainable geopolymer concrete production. Materials Today Sustainability. Elsevier Ltd; 2025; 29.
5. 5Liu J, Ren Y, Li Z, Niu R, Xie G, Zhang W, et al. Efflorescence and mitigation of red mud–fly ash–phosphogypsum multicomponent geopolymer. Constr Build Mater. 2024 Oct 18;448.
6. Chandralega V, Shanmugasundaram M, Stone D. Enhancing the performance of iron-based binders with seawater and CO_2 sequestration. Case Studies in Construction Materials. 2025 Jul 1;22.
7. Suprakash AS, Karthiyaini S, Shanmugasundaram M. A study on compressive strength of ultrafine graded fly ash replaced concrete and machine learning approaches in its strength prediction. Structural Concrete. 2022 Dec 7;23(6):3849–63.
8. Venkatesh V, Shanmugasundaram M. Enhancement of mechanical and microstructural characteristics of magnesium oxychloride cement with metasteatite. Case Studies in Construction Materials. 2024 Dec 1;21.
9. Vellapandi V, Muthusamy S. Influence of metasteatite on strength and porosity of magnesium oxychloride cement: An experimental and image processing approach. Revista Materia. 2024;29(4).
10. Konduru H, Karthiyaini S. Enhancing solidification in one-part geopolymer systems through alkali-thermal activation of bauxite residue and silica fume integration. Case Studies in Construction Materials. 2024 Dec 1;21.
11. Kaya K, Soyer-Uzun S. Evolution of structural characteristics and compressive strength in red mud-metakaolin based geopolymer systems. Ceram Int. 2016 May 1;42(6):7406–13.
12. Konduru H, Karthiyaini S, Shanmugasundaram M. Comparative study of silica fume and sodium silicate as replacement of active reactive silica in bauxite residue based geopolymer mortar. Case Studies in Construction Materials. 2025 Jul 1;22.
13. Lu J, Shen Y, Wang Y, Zhang H, Guan X, Zhu J, et al. In-situ wet carbonation activation of red mud waste for sustainable grout materials. Journal of Industrial and Engineering Chemistry. 2024 Aug 25;136:453–64.
14. Saranya V, Karthiyaini S, Stone D. Enhancement of strength and microstructural characterization in red mud-iron carbonate binders: Effects of CO_2 sequestration and oxalic acid concentration. Results in Engineering. 2025 Mar 1;25.
15. Simha B, Yeddula R, Somasundaram K. Effect of red mud proportion on the strength and microstructure of ferrosialate based geopolymer mortar. Indian Journal of Engineering & Materials Sciences. 2020; 27.
16. Ilahi K, Debbarma S, Mathew G, Inyang HI. Carbon capture and mineralisation using red mud: A systematic review of its principles and applications. Journal of Cleaner Production. Elsevier Ltd; 2024;473.
17. Haque MM, Ankur N, Meena A, Singh N. Carbonation and permeation behaviour of geopolymer concrete containing copper slag and coal ashes. Developments in the Built Environment. 2023 Dec 1;16.
18. Zhang M, El-Korchi T, Zhang G, Liang J, Tao M. Synthesis factors affecting mechanical properties, microstructure, and chemical composition of red mud-fly ash based geopolymers. Fuel. 2014 Oct 15;134:315–25.
19. Hu W, Nie Q, Huang B, Shu X, He Q. Mechanical and microstructural characterization of geopolymers derived from red mud and fly ashes. J Clean Prod. 2018 Jun 10;186:799–806.
20. Yang D, Wang P, Chen W, Liu L, Huang Y, Xiang X, et al. Effects of red mud, desert sand, and ground granulated blast furnace slag on the mechanical properties and microstructure of fly ash-based geopolymer. Constr Build Mater. 2025 Mar 21;468.
21. Rifaai Y, Yahia A, Mostafa A, Aggoun S, Kadri EH. Rheology of fly ash-based geopolymer: Effect of NaOH concentration. Constr Build Mater. 2019 Oct 30;223:583–94. Available from: https://www.sciencedirect.com/science/article/abs/pii/S0950061819316939
22. Chen K, Lin WT, Liu W. Effect of NaOH concentration on properties and microstructure of a novel reactive ultra-fine fly ash geopolymer. Advanced Powder Technology. 2021 Aug 1;32(8):2929–39. Available from: https://www.sciencedirect.com/science/article/abs/pii/S0921883121003058
23. Singh S, Aswath MU, S TB. Effect of silica on the properties of red mud based geopolymer mortar for synthesis of sustainable bricks. Journal of Building Pathology and Rehabilitation. 2024 Jun 1;9(1).
24. Li N, Unluer C. Rheology and phase formation of cement pastes incorporating CO_2-activated steel

slag as a supplementary cementitious material. Cem Concr Compos. 2025 Sep 1;162.

25. Wang S, Wang M, Liu F, Song Q, Deng Y, Ye W, et al. A review on the carbonation of steel slag: Properties, mechanism, and application. Materials, 2024;17.
26. Liu Y, Han Y, Shi T, Lv B, Zhang F, Zhou X. An innovative method for preparing nano steel slag powder and analysis of carbonation reaction mechanism toward enhanced CO_2 sequestration. Mater Lett. 2026 Jan 15;403.
27. Sankar K, Stynoski P, Al-Chaar GK, Kriven WM. Sodium silicate activated slag-fly ash binders: Part I – Processing, microstructure, and mechanical properties. Journal of the American Ceramic Society. 2018 Jun 2;101(6):2228–44.
28. Niklioć I, Marković S, Janković-Častvan I, Radmilović V V., Karanović L, Babić B, et al. Modification of mechanical and thermal properties of fly ash-based geopolymer by the incorporation of steel slag. Mater Lett. 2016 Aug 1;176:301–5.
29. Wang P, Chen P, Ming Y, Li Q, Dong X. In-depth insight into the effects of steel slag and calcium hydroxide on the properties of a fly ash–red mud geopolymer. Materials. 2024 Mar 1;17(6).
30. Harirchi P, Yang M. Exploration of carbon dioxide curing of low reactive alkali-activated fly ash. Materials. 2022 May 1;15(9).
31. Zheng D, Ni L, Zhang C, Yang S, Cui H. CO_2-mineralization strategy and mechanism of alkali-activated slag paste. Constr Build Mater. 2025 Feb 14;463.
32. Vinitha Mariyappan, Karthiyaini Somasundaram. The synergy of low-NaOH activation and carbon sequestration in sustainable red mud based geopolymer. Global NEST Journal, 2025 Oct 27; Available from: https://journal.gnest.org/publication/gnest_07964
33. Duraisamy S, Chaunsali P. Stabilization of red mud using mineral carbonation. Clean Eng Technol. 2025 Mar 1;25.
34. Liu S, Shen Y, Wang Y, Shen P, Xuan D, Guan X, et al. Upcycling sintering red mud waste for novel superfine composite mineral admixture and CO_2 sequestration. Cem Concr Compos. 2022 May;129:104497.
35. Huo B, Zhang Y, Wang D. Optimizing CO_2 capture property of alkali-activated ladle slag materials with sodium dodecyl sulfate. Powder Technol. 2025 Jan 15;449.
36. Ghasemzadeh Mousavinejad SH, Sammak M. An assessment of the effect of Na_2SiO_3/NaOH ratio, NaOH solution concentration, and aging on the fracture properties of ultra-high-performance geopolymer concrete: The application of the work of fracture and size effect methods. Structures, 2022 May 1;39:434–43. Available from: https://www.sciencedirect.com/science/article/abs/pii/S2352012422002132
37. Kiran Kumar NLN, Ramana Reddy I V. A study on the effect of NaOH molarity on flyash based self compacting geopolymer concrete. Mater Today Proc. 2023 Mar 21; Available from: https://www.sciencedirect.com/science/article/abs/pii/S2214785323011860
38. Wang P, Chen P, Ming Y, Li Q, Dong X. In-depth insight into the effects of steel slag and calcium hydroxide on the properties of a fly ash–red mud geopolymer. Materials. 2024 Mar 1;17(6).
39. Liu Z, Zhang D Wang, LI L, Wang J Xiang, Shao N Ning, Wang D Min. Microstructure and phase evolution of alkali-activated steel slag during early age. Constr Build Mater. 2019 Apr 20;204:158–65.
40. Li Z, Zhang J, Lei Z, Gao M, Sun J, Tong L, et al. Designing low-carbon fly ash based geopolymer with red mud and blast furnace slag wastes: Performance, microstructure and mechanism. J Environ Manage. 2024 Mar;354:120362.
41. Chen Y, Wu S, Huang H, Rao F, Yang L. Effect of calcium on the setting time and mechanical property of a red mud–blast furnace slag-based geopolymer. Materials. 2024 Sep 1;17(17).
42. Bernal SA, Provis JL, Rose V, Mejía De Gutierrez R. Evolution of binder structure in sodium silicate-activated slag-metakaolin blends. Cem Concr Compos. 2011 Jan;33(1):46–54.
43. Wang K, Hu S, Li Y, Xi Z, Qian J, Yuan B. Mechanical properties of carbonation-enhanced alkali-activated slag-solidified shield muck: temperature–humidity coupling effects. Applied Sciences (Switzerland). 2025 May 1;15(10).
44. Wang K, Zheng H, Li S, Sun Y, Ba H, Ma J. Study on carbonation behavior and carbon footprint of steel slag-calcium carbide slag-desulfurization gypsum composite system. Sci Rep. 2025 Dec 1;15(1).
45. Santos E.W.F., de Almeida N.D., Martins C.O.D., et al. Influence of exposure temperature variability on concrete degradation as a function of compressive strength and ultrasonic wave propagation velocity. Revista IBRACON de Estruturas e Materiais. 2024; 17(1). https://doi.org/10.1590/S1983-41952024000100004
46. Heshmat M, Amer I, Elgabbas F, Khalaf MA. Effect of binder and activator composition on the characteristics of alkali-activated slag-based concrete. Sci Rep. 2024 Dec 1;14(1).
47. Mavroulidou M, Sanam I, Mengasini L. Mechanical and durability performance of alkali-activated slag cement concretes with carbonate and silicate activators. Sustain Chem Pharm. 2023 Apr 1;31.
48. Shilar FA, Ganachari S V., Patil VB, Khan TMY, Dawood Abdul Khadar S. Molarity activity effect on mechanical and microstructure properties of

geopolymer concrete: A review. Case Studies in Construction Materials. 2022 Jun 1;16.

49. Amran M, Al-Fakih A, Chu SH, Fediuk R, Haruna S, Azevedo A, et al. Long-term durability properties of geopolymer concrete: An in-depth review. Case Studies in Construction Materials. 2021 Dec 1;15.
50. Yong-Sing N, Yun-Ming L, Abdullah Mmab, Hui-Teng N, Bayuaji R. Ladle furnace slag replacement on the flexural strength of thin fly ash geopolymer. European Journal of Materials Science and Engineering. 2020 Sep 20;5(3):133–44. Available from: http://ejmse.ro/articles/05_03_03_EJMSE-20-105.pdf
51. Zhang M, He M, Pan Z. Inhibition of efflorescence for fly ash-slag-steel slag based geopolymer: Pore network optimization and free alkali stabilization. Ceram Int. 2024 Nov 15;50(22):48538–50.
52. Li J, Liu X, Cai C, Li F, Jin H, Zhang S, et al. Microstructure, strength development mechanism and CO2 emission assessments of molybdenum tailings collaborative fly ash geopolymers. Case Studies in Construction Materials. 2024 Dec 1;21.
53. Jun Y, Han SH, Kim JH. Performance of CO_2-cured alkali-activated slag pastes during curing and exposure. Int J Concr Struct Mater. 2023 Dec 1;17(1).
54. Venkatachalam S, Somasundaram K. Adverse effect on the strength and microstructural characteristics of iron-based binders under the influence of initial atmospheric exposure before CO_2 curing. Advances in Science and Technology Research Journal. 2026 Jan 1;20(1):222–35.
55. Sifueli Malisa A, Hamisi Chengula D. Efflorescence formation mechanism and control for geopolymer paste specimens made from natural pozzolan and calcium hydroxide binders. American Journal of Polymer Science and Technology. 2023 Jun 21.
56. Han W, Lv Y, Wang S, Qiao J, Zou C, Su M, et al. Effects of Al/Na and Si/Na molar ratios on the alkalinity of metakaolin-based geopolymer pore solutions. Materials. 2023 Mar 1;16(5).
57. Zhang X, Wang X, Zhan Q, Song C. Carbonation reaction properties and reaction mechanisms of red mud under different carbon dioxide pressures. J Environ Chem Eng. 2024 Jun 1;12(3).
58. Shi Y, Zhang Z, Sang Z, Zhao Q. Microstructure and composition of red mud-fly ash-based geopolymers incorporating carbide slag. Front Mater. 2020 Nov 6;7.
59. Hao X, Liu X, Zhang Z, Zhang W, Lu Y, Wang Y, et al. In-depth insight into the cementitious synergistic effect of steel slag and red mud on the properties of composite cementitious materials. Journal of Building Engineering. 2022 Jul 15;52:104449. Available from: https://www.sciencedirect.com/science/article/abs/pii/S2352710222004624
60. Temuujin J, van Riessen A, Williams R. Influence of calcium compounds on the mechanical properties of fly ash geopolymer pastes. J Hazard Mater. 2009 Aug 15;167(1–3):82–8.
61. Wang Y, Zhang J, Liu J, Fan D, Qu H, Zhou L, et al. Effects of different calcium sources on mechanical properties of metakaolin geopolymers. materials. 2024 May 1;17(9).
62. Das SK, Shrivastava S. Influence of molarity and alkali mixture ratio on ambient temperature cured waste cement concrete based geopolymer mortar. Constr Build Mater. 2021 Sep;301:124380.
63. Shi X, Lyu S, Wang Q, Xiao J, Li Y. Experimental study on the effect of carbonate ions on ITZs of geopolymeric recycled concrete. Constr Build Mater. 2024 Oct 4;446.
64. Liu Y, Zhuge Y, Chen X, Duan W, Fan R, Outhred L, et al. Micro-chemomechanical properties of red mud binder and its effect on concrete. Compos B Eng. 2023 Jun;258:110688.
65. Sufian Badar M, Kupwade-Patil K, Bernal SA, Provis JL, Allouche EN. Corrosion of steel bars induced by accelerated carbonation in low and high calcium fly ash geopolymer concretes. Constr Build Mater. 2014 Jun 30;61:79–89.
66. Guo S, Wang R, Zhang Y, Zhang R, Zheng D, Ren J, et al. Comparative analysis of CO_2 Resistance on NaOH-Activated and $Na_2C_2O_4$ + $Ca(OH)_2$-Activated Geopolymers. ACS Omega. 2025 May 6;10(17):17483–94.
67. Pan H, Zhang B, Cao J, Yang Z, Chen J, Zhao X, et al. Performance and alkalinity control in geopolymer coral aggregate concrete via experiments and machine learning. Sustainable Materials and Technologies. 2025 Oct 1;45:e01555. Available from: https://www.sciencedirect.com/science/article/abs/pii/S2214993725003239